Ecological Applications, 31(5), 2021, e02339

Rapid deforestation of a coastal landscape driven by sea-level rise and extreme events

Emily A. Ury [1,3], Xi Yang [2], Justin P. Wright [1], and Emily S. Bernhardt[1]

[1]*Department of Biology, Duke University, Box 90338, Durham, North Carolina 27708 USA*
[2]*Department of Environmental Sciences, University of Virginia, Charlottesville, Virginia 22904 USA*

Citation: Ury, E. A., X. Yang, J. P. Wright, and E. S. Bernhardt. 2021. Rapid deforestation of a coastal landscape driven by sea-level rise and extreme events. Ecological Applications 31(5):e02339. 10.1002/eap.2339

Abstract. Climate change is driving ecological shifts in coastal regions of the world, where low topographic relief makes ecosystems particularly vulnerable to sea-level rise, salinization, storm surge, and other effects of global climate change. The consequences of rising water tables and salinity can penetrate well inland, and lead to particularly dramatic changes in freshwater forested wetlands dominated by tree species with low salt tolerance. The resulting loss of coastal forests could have significant implications to the coastal carbon cycle. We quantified the rates of vegetation change including land loss, forest loss, and shrubland expansion in North Carolina's largest coastal wildlife refuge over 35 yr. Despite its protected status, and in the absence of any active forest management, 32% (31,600 hectares) of the refuge area has changed landcover classification during the study period. A total of 1,151 hectares of land was lost to the sea and ~19,300 hectares of coastal forest habitat was converted to shrubland or marsh habitat. As much as 11% of all forested cover in the refuge transitioned to a unique land cover type—"ghost forest"—characterized by standing dead trees and fallen tree trunks. The formation of this ghost forest transition state peaked prominently between 2011 and 2012, following Hurricane Irene and a 5-yr drought, with 4,500 ± 990 hectares of ghost forest forming during that year alone. This is the first attempt to map and quantify coastal ghost forests using remote sensing. Forest losses were greatest in the eastern portion of the refuge closest to the Croatan and Pamlico Sounds, but also occurred much further inland in low-elevation areas and alongside major canals. These unprecedented rates of deforestation and land cover change due to climate change may become the status quo for coastal regions worldwide, with implications for wetland function, wildlife habitat, and global carbon cycling.

Key words: climate change; coastal forests; deforestation; ghost forest; remote sensing; salinization; saltwater intrusion; sea-level rise; wetlands.

Introduction

Climate change is transforming landscapes around the world, and in the case of many coastal regions, change is occurring faster than ecosystems are able to adapt. Sea-level rise may inundate up to 76,000 km^2 of land in the conterminous United States alone (Haer et al. 2013). Around the world, coastal landscapes are experiencing inundation, saltwater intrusion, coastal storms, and other extreme events associated with anthropogenically driven climate change (Meehl et al. 2007, Church et al. 2013, Cloern et al. 2016). Shoreline loss and marsh migration are well-documented ecosystem responses to sea-level rise (Wasson et al. 2013, Fagherazzi et al. 2019); however, in low-lying coastal plain landscapes, the impacts of sea-level rise and saltwater intrusion are not confined to the coastal margins (Manda et al. 2014, White and Kaplan 2017, Bhattachan et al. 2018). Low-lying coastal landscapes often support forested wetland vegetation; these tree-dominated communities are not well adapted to permanently saline conditions and their response to sea-level rise is not well understood (Munns and Tester 2008). The Atlantic Coastal Plain of North America is characterized by bottomland forested wetlands and fringing marshes (Brinson 1991). These wetlands are important wildlife habitat, provide valuable ecosystem services, and are globally important carbon sinks (Brinson 1991, Duarte et al. 2013, Spivak et al. 2019).

Historic land use of coastal plain regions has resulted in a landscape that is particularly vulnerable to sea-level rise. The construction of drainage ditches for agriculture and channelization for navigation has increased the connectivity of the landscape interior to saline coastal waters (Bhattachan et al. 2018). Salt moves up-gradient because of diffusion, and its effects on vegetation often precede other visible evidence of sea-level rise (Tully et al. 2019). Land drainage for agriculture and forestry

Manuscript received 6 March 2020; revised 16 September 2020; accepted 27 October 2020. Corresponding Editor: John Christopher Stella.
[3] E-mail: ury.emily@gmail.com

has further accelerated the effects of sea-level rise by inducing subsidence of the ground's surface through oxidation of previously anoxic soils (Holden et al. 2004). As a result, modification of coastal plain landscapes has altered the pathways and spatial patterns of ecological change.

Extreme events further complicate our attempts to measure and predict salinization in coastal landscapes, and increases in the number of extreme events (storms, drought, fire, and flooding) are an additional impact of climate change (Meehl et al. 2007). Without accounting for disturbance events, elevation is the primary determinant of the forest–marsh boundary and the rate of lateral wetland retreat (Schieder and Kirwan 2019). However, disturbance events, which are prevalent in coastal environments, exert control on the timing and pace of lateral retreat. Both coastal storms and droughts can increase the inputs of saltwater into coastal interiors (Tully et al. 2019). Major coastal hurricanes can reverse the flow of water in coastal creeks and canals and deliver sea spray far inland. Droughts in these low-elevation landscapes can allow wind tides to mix saltwater miles upstream through stagnant creeks and canals. These disturbance-driven inputs of marine salts exacerbate the gradual processes associated with sea-level rise, leading to an "ecological ratchet" effect, whereby each salt-loading disturbance enhances the potential for an ecosystem state change to occur in response to chronic sea-level rise (Fagherazzi et al. 2019, Hillebrand and Kunze 2020). The location and timing of extreme events may thus determine much of the spatiotemporal patterns of coastal landscape change.

One of the most striking transitions observed in coastal landscapes in recent decades is the rapid mortality of entire stands of trees, or "ghost forests," characterized by a high density of standing dead trees and indicating recent, rapid, and synchronous tree mortality (Kirwan and Gedan 2019). Recent work in coastal forests around the Chesapeake Bay describes a fringe of ghost forest at the transition between healthy trees and migrating salt marshes (Schieder and Kirwan 2019). Indeed, we might expect this ghost forest fringe to be the natural outcome of marsh migration in response to sea-level rise marking the inland extent of saline conditions. Coastal trees can withstand periodic salinity exposure, but the osmotic stress of chronically saline conditions will impede germination and eventually lead to tree mortality (Munns and Tester 2008, Kirwan and Gedan 2019). In this study, we seek to understand the rates and spatial patterns of ghost forest formation and other pathways of coastal vegetation change in service of understanding the drivers and extent of change in coastal plain landscapes.

Remote sensing is valuable for understanding landscape-scale response to changing environmental conditions. Numerous remote sensing platforms, sensors, and techniques have been used to study vegetation and vegetation change. Among them, the Landsat satellite record holds one of the longest-running data sets that can be applied to look at change over time (Adam et al. 2010, Kennedy et al. 2014). Here, we demonstrate the utility of remote sensing time series for understanding ecosystem responses to global climate change. We measured the magnitude, the trajectory, and the spatial distribution of land and forested wetland loss throughout this vulnerable coastal landscape over the last 35 yr. We asked three questions. First, what proportion of the land area and of forested wetlands were lost? Second, to what extent do losses of land and forest occur beyond the coastal fringe? Third, are the temporal trends in land and forest loss driven by gradual sea-level rise or by extreme events?

Methods

Study location

The Atlantic Coastal Plain of the United States is experiencing rapid rates of relative sea-level rise—estimated 3–4 mm/yr compared with global mean sea-level rise of 1–2 mm/yr (Douglas and Richard Peltier 2002, Church et al. 2013). Protected by a string of barrier islands, the Coastal Plain of North Carolina is characterized by large areas of intact coastal forest at low elevation and with little topographic relief. The Alligator River National Wildlife Refuge (NWR) is the second largest protect area in the state of North Carolina and an ideal place to study the pace and drivers of vegetation change because of the distinct lack of development, forestry, and other anthropogenic activities. The median elevation of our study area is less than 0.5 m above sea level. Soils are largely peat based and poorly drained with water table depth ranging from −20 cm to +10 cm above the ground (Poulter 2005). The region was also extensively drained for agriculture and forestry during the mid-20th century resulting in a dense network of ditches and canals across the landscape (approximately 4 km of drainage length per square-kilometer area; Poulter et al. 2008).

Vegetation includes high and low pocosins (poorly drained peatlands of the southeastern United States characterized by dense shrubby vegetation), freshwater and brackish marshes (mainly *Caladium jamaicense* and *Spartina* sp.), hardwood swamps (various *Quercus* species, *Acer rubrum* and *Liquidambar styraciflua*), and bald cypress (*Nyssa sylvatica*) (Brinson 1991). The Refuge was established in 1984 to protect the unique pocosin wetland habitat and associated wildlife, including several endangered species: the red wolf, the red-cockaded woodpecker, and the American alligator as well as the globally threatened Atlantic white cedar (*Chamaecyparis thyoides*) ecosystem. The specific region of interest includes most of Alligator River NWR and surrounding natural lands, but excludes major roads, water bodies, agricultural land, and the Dare County Bombing Range (Fig. 1). The study area was affected by the Pains Bay Fire during the summer of 2011 and Hurricane Irene, which made landfall in August of the same year. The fire affected approximately 97 km^2 within the 615-km^2

FIG. 1. Location of study region (shaded in green) in Eastern North Carolina.

refuge (U.S. Fish and Wildlife Service Southeast Region Fire Management Organization 2011) and the hurricane brought a 2-m storm surge to the nearest gauge station in the Pamlico Sound (National Weather Service Advanced Hydrologic Prediction Service 2016). The storm surge was said to have inundated the Refuge with water cresting over Highway 264, more than 2 km inland from the coast (S. Lanier, *personal communication*).

Image preprocessing

Google Earth Engine (GEE) was used to generate annual composite images using scenes from the Landsat Satellite record from the U.S. *Geological Survey* (USGS). We used images from three of Landsat's instruments, Landsat 5 Thematic Mapper (TM), Landsat 7 Enhanced Thematic Mapper Plus (ETM+), and Landsat 8 Operational Land Imager (OLI) to span the period from 1985 to 2019. For each imager, only the atmospherically corrected Tier 1 Surface Reflectance product was used. All available scenes of the study region were clipped to apply a water mask generated from the same year's annual water occurrence values from the JCR Yearly Water Classification History (Pekel et al. 2016). For each year we used both a winter (November–March) and summer (May–September) composite to generate the input to our classifier. The composite for each season is generated from the stack of images within the seasonal window, clouds and cloud shadow pixels were masked out, and pixels were reduced to the median reflectance of each band. Each composite was inspected for clouds and other artifacts or distortions, and if present, the contributing images were removed individually. For some years, a suitable composite was not achieved and thus left out of the analysis. The two seasonal composites were combined such that the input for the classifier contains 12 bands in total, 6 (blue, green, red, NIR, SWIR1, and SWIR2) from each season.

Land cover classification

Training data for vegetation classes were collected from Google Earth imagery (collected 24 March 2017, 10 cm RGB [Red, Green, Blue]) and from North

Carolina orthophotos available from the USGS (collected 28 February 2012 and 11 April 2010, 15 cm RGB). Randomly generated validation points (n = 500) were classified by hand with additional points added to improve spatial coverage of all classes. Vegetation was classified into the following categories: pine, deciduous, shrub, marsh, and ghost forest. Ghost forest pixels were characterized by the density of visibly dead trees present in the high-resolution imagery. Ghost forest stands are easily distinguished due to the lack of branches on snags and the presence of fallen tree trunks. Because the orthophotos were collected in the winter, it was easy to distinguish between the pine and deciduous classes (see Fig. 2). For some analyses, pine and deciduous classes are combined into one class: "forested wetland." There is no need to distinguish between forested wetland and upland forest in this study because the entire region is considered wetland (either woody or emergent herbaceous) according to the USGS National Land Cover Database (Yang et al. 2018). The shrubland class consists of mixed scrub-shrub type vegetation, with some herbaceous vegetation visible and large trees mostly absent. The marsh class consists of either freshwater or saltwater herbaceous species. Because of the Pains Bay Fire of 2011 that affected a large portion (16%) of the study area, a burn category was also included in the 2012 imagery demarcating areas that burned beyond reasonable recognition of the vegetation. In 2012, large areas of pine trees exhibited browning needles, most likely because of drought or fire. These trees largely recovered in subsequent years, but the unusual coloring reduced the accuracy of the classifier, so an addition class was added in 2012 (called "dry pine"), which was then later merged back into the pine class for analysis.

We used a random forest decision tree algorithm (Breiman 2001) to classify the composited inputs for each year of training data sets (2010, 2012, and 2017). Our use of spectral signatures for detecting and classifying vegetation follows standard approaches of remote sensing land cover land use classification (Asner 1998, Ustin et al. 2009, Ustin 2013). The reflectance of bare tree trunks is distinct from both live trees and understory vegetation, allowing us to detect ghost forests as a unique class. Accuracy assessment was performed on these years using k-fold cross-validation with five groups. The classifier that was trained on 2017 data was then applied to the other annual composites from Landsat 8 OLM (2015–2019). The classifier that was trained on 2010 data was used to classify the composites from Landsat 5 TM (1985–2011).

Statistical analysis

Statistical analyses were run in the R statistical computing environment (R Development Core Team 2013). Classification was done using the R package "randomForest" (Liaw and Wiener 2002) with Ntree and mtry default values. Other R packages used for data transformation and visualization included "raster" (Hijmans 2019), "rgdal" (Bivand et al. 2019), "alluvial" (Bojanowski and Edwards 2016), and the *Tidyverse* (Wickham et al. 2019). We used bivariate logistic regression (glm() function, family = binomial) to determine the influence of topographic characteristics on forest loss and ghost forest formation. In these models, forest loss is a binary response variable indicating if a pixel was classified as forest at the start of the study period but not at the end. Environmental predictors for channels and coastline were generated by calculating a simple linear distance raster in R using tools from the "raster" package and derived from the National Hydrography Data Set (NHD) flow lines for the State of North Carolina and 30-m resolution Digital Elevation Model (DEM) from the USGS. A bootstrapping approach with random draws of 1,000 pixels using a 500-m exclusionary buffer was used to generate model input data as a means of reducing spatial autocorrelation among covariates.

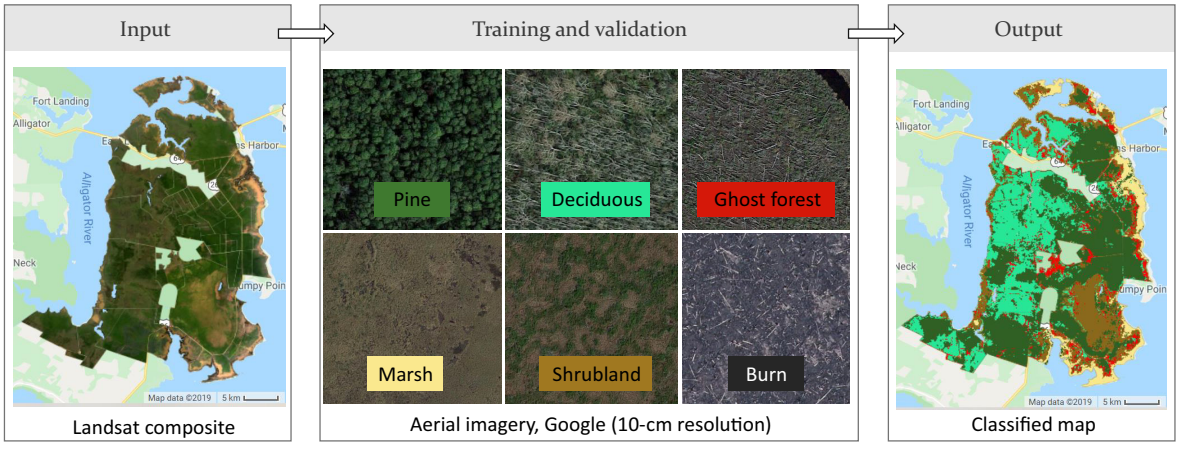

FIG. 2. Classification schematic and examples of each vegetation class as seen in Google Earth imagery.

Results

The results from our classification demonstrate that it is possible to detect coastal ghost forests using Landsat imagery. The overall accuracy for all five classes was 92.2% for the Landsat 8 classifier, 82.5% for the Landsat 7 classifier, and 82.3% for Landsat 5 classifier. The average producer accuracy and user accuracy for the ghost forest class is 88.8% and 85.5%, respectively. In the orthophotos used for training data, each point characterized as ghost forest contained approximately 20–40 visible snags or fallen tree trunks per Landsat pixel (about 220–440 dead trees per hectare). In a random sample of Landsat pixels classified as ghost forest, the mean number of snags and fallen trunks per pixel was lower (mean = 13, n = 50), which is likely because of bare ground reflectance, which also contributes to the spectral characteristics of a ghost forest pixel. This may suggest a slight overfitting of the ghost forest class; however, the overall accuracy for this class is still quite good (see Appendix S1: Table S1). We assume that the overall accuracies are a good approximation of the accuracy of each map produced with the respective classifier. Lower accuracy from the older imagery is due in part to a lack of validation points within the ghost forest class (there simply were not as many ghost forests present at that time on which the classifier could be trained). We found that using both a winter and summer composite image greatly enhanced the classifier's ability to distinguish between the pine, deciduous, and ghost forest categories; in summer the pine/deciduous distinction is more difficult to parse and in winter the deciduous/ghost forest signatures are similar, but combining summer and winter reflectance enables us to distinguish between all three. Overall, pine, deciduous, and marsh were the most successfully distinguishable classes for the classifiers and shrub and ghost forest were more difficult to parse out (see complete confusion matrices in Appendix S1: Tables S1–S4).

In this 99,347-hectare (ha) study area, 77% (76,575 ha) was forested wetland in 1985. Over 35 yr, the refuge has lost 1,151 ha of land (1.2%) to open water and had a net loss in forest cover of 15,811 ha (Table 1). Most strikingly, of the 76,575 ha that were forest in 1985, 21,097 ha (27.6%) transitioned to either shrub, marsh, ghost forest, or open water by 2019. In fact, only 69.2% percent of this protected wildlife refuge has not experienced a vegetation transition over the last 35 yr (shown in light gray in Fig. 3A). Of the forest classes that transitioned to nonforest classes, 40.8% (8,616 ha) went through a detectable ghost forest stage at some point during the study period (these are the pathways shown in red in Fig. 3B). The majority (17,115 ha, 81%) of the forested area that transitioned is now categorized as shrubland. Parts of the Refuge have experienced forest regrowth (mainly from shrubland) totaling 5,287 ha. The marsh class has grown about 7% over the study period; however, its position on the landscape has shifted: marshes are moving inland to areas that were shrub and forest as the shoreline retreats. The conversion to marsh is occurring both with and without a ghost forest transition state (Fig. 3B), which may indicate the relative contributions of multiple mechanisms driving vegetation change.

The spatial distribution of change within the refuge is most heavily concentrated along the coasts, and the eastern side along the sound is more severely affected than the western coast on the Alligator River (see the map in Fig. 3A and histogram in Fig. 4D). The distribution of forest loss is concentrated on the eastern side of the refuge; however, 59% of forest loss is occurring in the interior part of the landscape (more than 1,000 m from either coast). The distribution of forest loss is more concentrated at low elevations (Fig. 4E). The distribution of forested pixels and forest loss based on distance to channel is heavily right skewed, owing to the prevalence of channels in this landscape (Fig. 4F).

Each of the topographic predictors in the spatial models of forest loss and ghost forest formation (binary response variables) are statistically significant (P values <0.001) drivers of these transitions except for distance to channel on ghost forest formation (P value = 0.11) (Fig. 5). The spatial autocorrelation of some variables (e.g., topography) violates the assumption of independent observations, and reduces the effective sample size. However, using random subsets of the data reduces the effect of autocorrelation (Moran's I is reduced for each model from 0.86/0.71 to 0.39/0.21), and the subsequent impact on the P values is negligible. Distance to the sound (the eastern shore of the refuge) was the strongest predictor of both forest loss and ghost forest formation compared with elevation and distance to a channel. We standardized the predictor variables in the linear model such that the slope coefficients may be compared to determine the relative strength of each predictor on the outcome of a forested pixel. The coefficient estimate for distance to the sound was −0.839 (95% confidence interval [CI] −1.01 to −0.669) for forest loss and −0.906 (95% CI −1.12 to −0.689) for ghost forest formation. Negative coefficient estimates indicate that forests closer to the coast are more likely to undergo these types of transitions. The coefficient estimate for elevation was −0.673 (95% CI −0.862 to −0.485) for forest loss and −0.677 (95% CI −0.928 to −0.426) for ghost forest

Table 1. Summary of the net change for each vegetation class (in hectares).

Class	1985	2019	Net change
Pine	27,483	20,205	−7,279
Deciduous	49,092	40,560	−8,532
Ghost forest	66	2,051	+1,985
Shrub	13,798	25,850	+12,052
Marsh	8,907	9,530	+623
Open water	0	1,151	+1,151

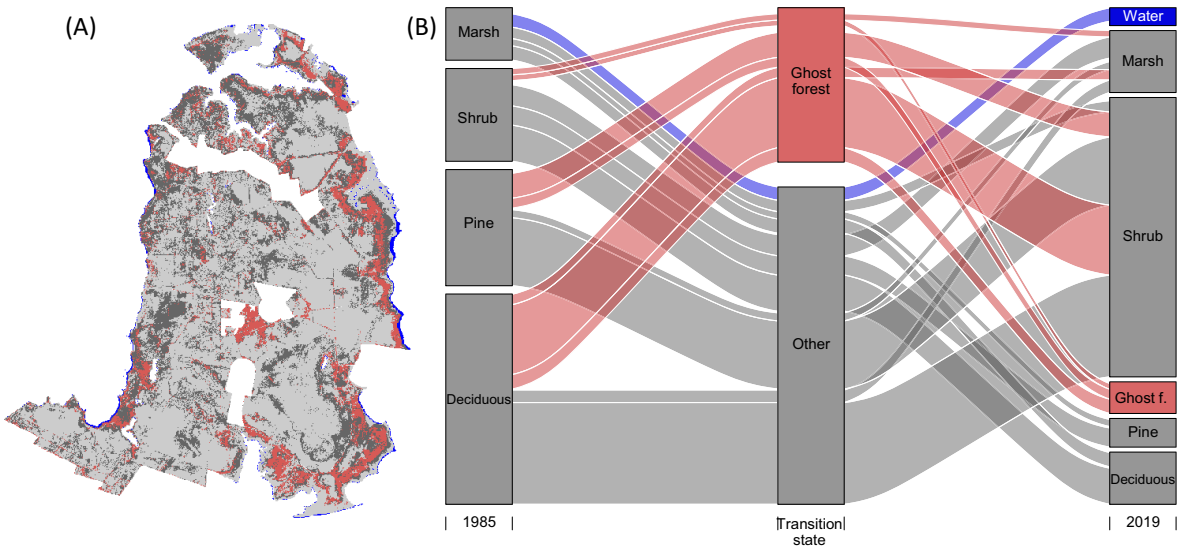

FIG. 3. (A) Map of study region areas that have undergone change since 1985. Blue denotes the conversion from land to open water, red indicates transition through ghost forest at any point in time, dark gray are all other changing areas, and light gray indicates no change. (B) For the changing pixels only, the alluvial plot shows the relative frequency of the various transition pathways.

formation; forests at lower elevation are more likely to transition. The coefficient estimate for distance to a channel was +0.239 (95% CI 0.098–0.380) for forest loss and −0.170 (95% CI −0.357 to 0.018) for ghost forest formation. The effects of proximity to a channel are of lesser magnitude and are inconsistent: forested wetlands are less likely to be lost alongside channels, but the effect on ghost forest formation is not statistically significant. We speculate that adjacency to a channel may be associated with less drought risk for much of the area and for the possibility of event-based salinization and mortality for trees alongside canals nearest to the sound. The ghost forest response variable indicates a ghost forest was detected at any time during the time series but modeling each year individually shows that the relative importance and even the direction of these relationships vary across the time series (see Appendix S1: Fig. S1).

The changing areas of Alligator River NWR are shown in Fig. 6A for the entire period of study. The steady loss of land to open water is apparent in the blue wedge along the *x*-axis. In contrast to the linear pace of land conversion to open water, the vegetation classes fluctuate over time (10–20% of this fluctuation maybe attributed to classification error). The forested area (pine and deciduous classes combined) is declining over time and the shrubland is expanding. The formation of ghost forest happened most dramatically between 2011 and 2012, and although the rates of ghost forest formation remain high (Fig. 6B), the total area of ghost forest on the landscape declines after peaking in 2012. We address the possible reasons for the observed timing of ghost forest formation in the discussion, but the direct hit of Hurricane Irene in the study region is a notable factor.

DISCUSSION

Despite its protected status and the absence of any timber management, more than 19,000 ha of freshwater wetland forests have been lost from the Alligator River NWR since 1985. We determined that 30.8% of the landscape in our study region has experienced a transition of vegetation type within the last 35 yr. The magnitude of forest cover lost is far greater than the amount of land lost outright to open water over the same time period (~1,150 ha). Forest loss was concentrated in a band approximately 1 km inland from the coastal margin, and was greater in extent on the eastern, more saline shores of the Albemarle-Croatan-Pamlico Sound than on the western side along the Alligator River estuary. This forested wetland loss was not just on the shoreline, with more than half of all forest loss occurring in the interior of the refuge. Although the trajectory of land loss in the study area was linear, forest loss was not. Instead, most of the ghost forest formation occurred within the last decade following a series of extreme events including 5 yr of drought (2007–2011), a major fire, and Hurricane Irene (both in 2011).

This analysis is the first reported attempt to use remote sensing to map the spatial and temporal distribution of coastal ghost forests. We were successful at training a classification algorithm to detect this unique transition state. Our analysis shows that ghost forests are both a prevalent and a transient feature in the Coastal Plain of North Carolina. We were surprised by the rapidity with which formerly forested patches transitioned through the ghost forest phase into shrublands or marsh, with pixels typically classified as ghost forests for no more than a few years. A portion (26.1%) of the

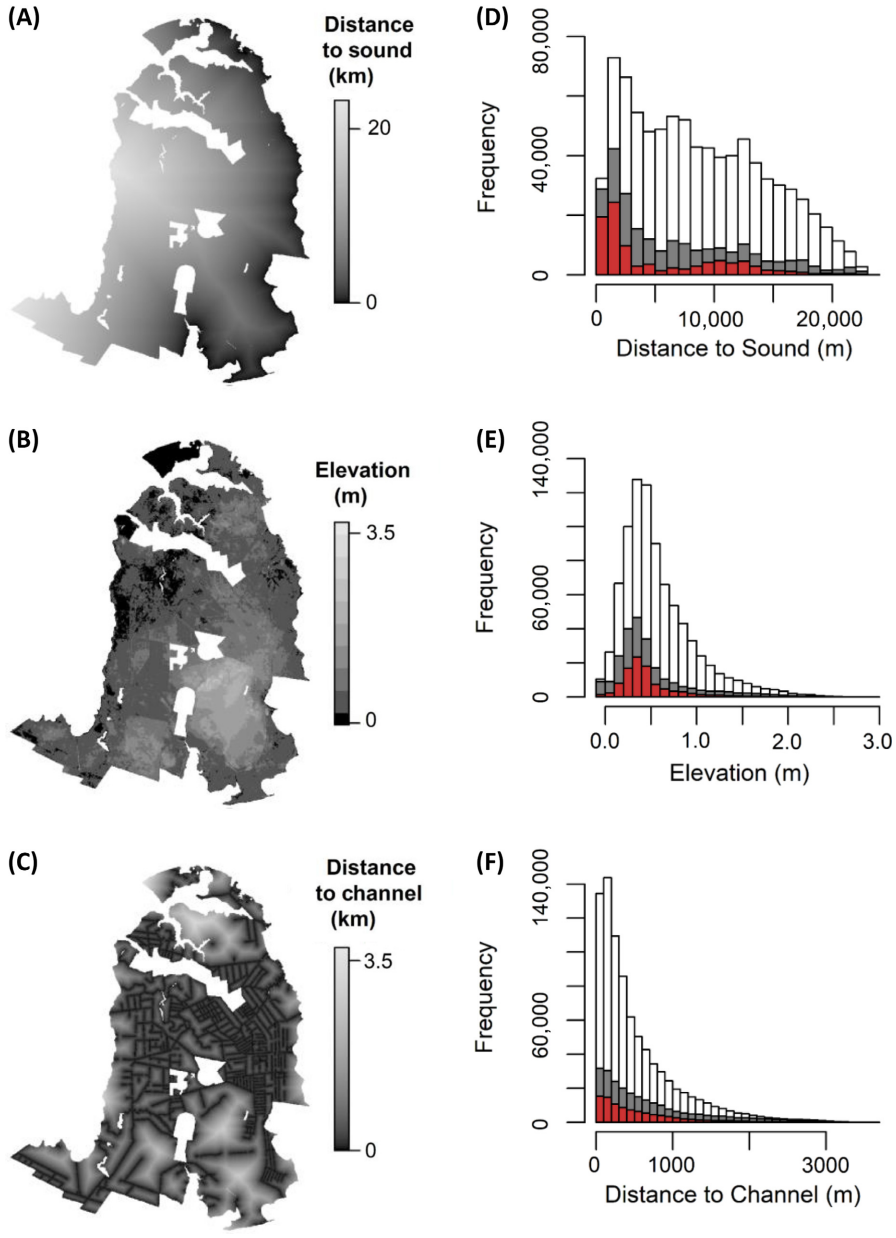

FIG. 4. Maps of spatial predictors (A) distance to the sound, (B) elevation above mean sea level, and (C) distance to a channel. Histograms of the distribution of forested pixels (white), pixels where forest cover was lost (gray), and forest pixels that went through a ghost forest state (red) across the same topographical parameters are shown in (D)–(F).

ghost forests detected earlier in the record (before 2010) have returned to a forested state, but for most pixels the ghost forest stage appears to represent a transition to nonforested vegetation cover. Most of the ghost forests have become shrublands. We do not yet know whether the resulting increase in scrub-shrub wetlands represents an expansion of native plant communities that are characteristic of this habitat type or the creation of novel or random assemblages. The impact of these widespread ecosystem transitions on biodiversity and community composition deserves further study. A portion of forests becoming scrub-shrub does not transition through a ghost forest stage, which we attribute to gradual tree mortality and forest thinning without replacement rather than mass tree mortality events that lead to large numbers of standing dead trees. The shrubland land cover type is rapidly expanding in area and represents a major shift in ecosystem structure for which the consequences for carbon storage and other ecosystem services have not yet been quantified.

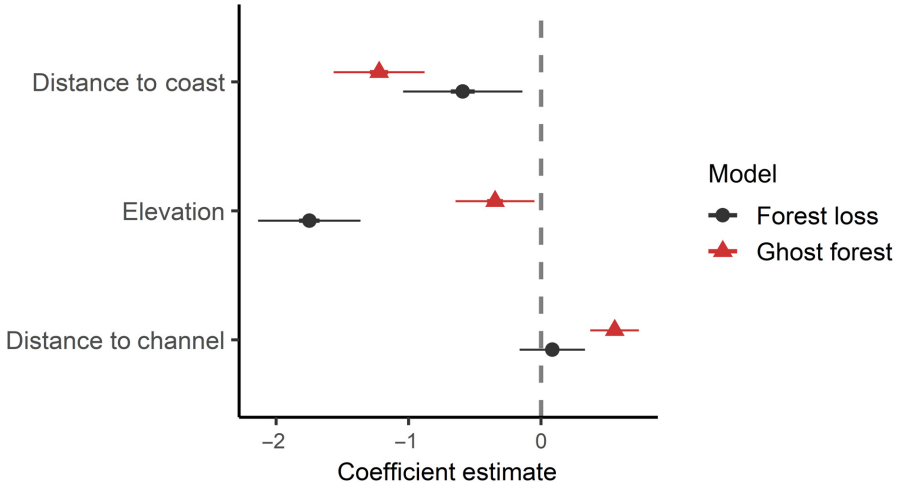

FIG. 5. Distance to the sound is the dominant controlling factor of ghost forest formation (red triangles) and forest loss (black dots) followed by elevation and distance to channel (coefficient estimates shown with 95% confidence interval). Predictors with negative coefficients increase the risk of forest loss and ghost forest formation.

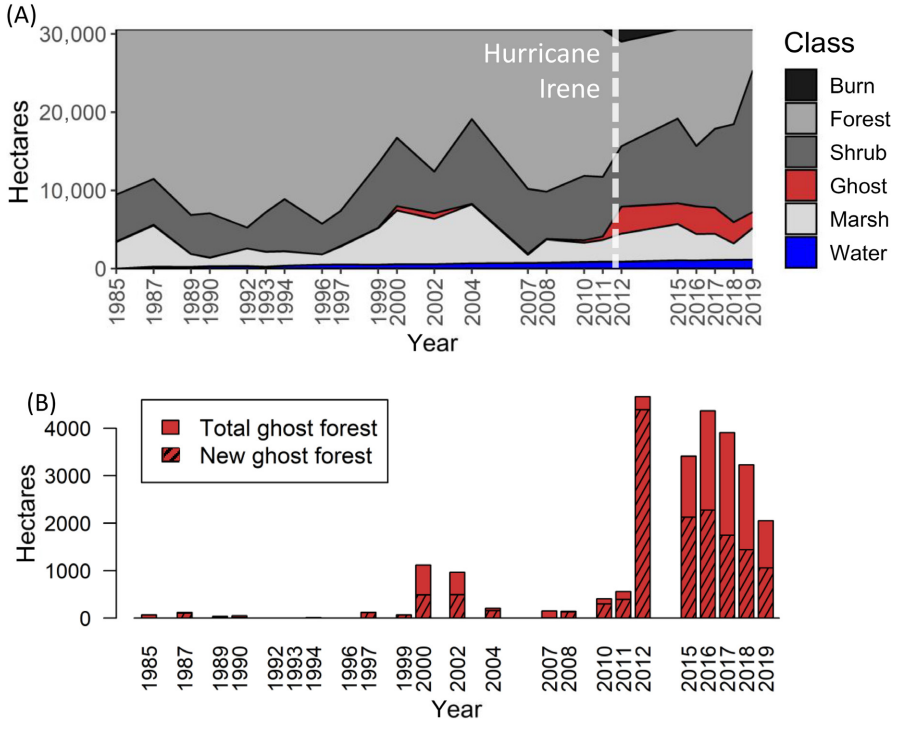

FIG. 6. (A) Changing areas of the Alligator River National Wildlife Refuge (pine and deciduous classes were combined to "forest," and data were interpolated linearly across years missing data). The formation of ghost forest (red) shows a marked increase following Hurricane Irene. The Pains Bay Fire (summer 2011) left a large burn scar on the land that was visible in the 2012 imagery. (B) Extent of ghost forest observed each year with the hashed area representing areas not classified as ghost forest in the previous year and considered newly formed.

If sea-level rise were the primary driver of forested wetland loss, we would expect to see a linear rate of vegetation change and confinement of forest loss to shorelines. Instead, the spatial distribution of forested wetland loss appears more consistent with saltwater intrusion, and the timing suggests that extreme events are leading to forest mortality. In this landscape of low topographic relief and shallow groundwater, all hydrologically connected areas are potentially vulnerable to saltwater intrusion (Bhattachan et al. 2018, Zhang et al. 2018,

2019). Marine salts move inland as a result of diffusion and wind tides during droughts as well as during hurricane storm surges (Manda et al. 2014, 2018, Tully et al. 2019). The greatest period of ghost forest formation (2011–2012) followed Hurricane Irene, which arrived after nearly 5 yr of drought. Although vegetation may still be in the recovery phase following these more recent disturbances, some areas may not recover, having been pushed too far into a new state. The combination of these two stressors may have been responsible for the increase in ghost forest formation, an interaction effect that may become more prevalent in the future as climate change is leading to an increased frequency of extreme events (Meehl et al. 2007, Miao et al. 2009).

Our study area represents only a small fraction of the 97,000 km^2 of palustrine forested wetland in the coastal plain of eastern North America (National Oceanic and Atmospheric Administration [NOAA] 2010). By definition, these are low-lying coastal forests that are vulnerable to rising sea levels, saltwater intrusion, and coastal storm damage. If the rates of change observed in this study are consistent across the entire North Atlantic Coastal Plain, climate deforestation could have already resulted in a tremendous loss of these unique ecosystems from North America. Field surveys have already documented dramatic losses of freshwater forested wetlands in the region (Desantis et al. 2007, White and Kaplan 2017, Kirwan 2019, Taillie et al. 2019*a*, Ury et al. 2020). There is no reason to expect the east coast of North America to be an outlier in the vulnerability of its coastal forested wetlands. Indeed, a recent analysis suggested that parts of northern Europe, Chile, Australia, and particularly southeast Asia will experience the most severe effects of climate-driven losses of coastal plain wetlands (Blankespoor et al. 2014).

The extensive transformation of coastal plain vegetation we observed has taken place despite the protected status of the refuge and active management to maintain endemic and rare plant communities (Laderman 1989, Poulter et al. 2008). In many other coastal plains, historic drainage and deforestation have confined endemic forested wetlands to the limited areas where drainage is very costly. These remnant wetland forests, which maybe the last stronghold and seedbanks for threatened species such as the Atlantic white cedar (*Chamaecyparis thyoides*) (Laderman 1989), may now be especially vulnerable because of their landscape position. Already the loss of forested freshwater wetlands in coastal North Carolina has been linked to declines in bird diversity (Taillie et al. 2019*b*).

Because freshwater forested wetlands are known to be important global carbon sinks (Brinson 1991), their conversion to shrublands may create positive feedbacks to climate change (Duarte et al. 2013, Spivak et al. 2019). Forested wetlands have far higher aboveground biomass than the shrublands that replace them (Kirwan and Gedan 2019). The effects of salinization on the carbon stocks stored in freshwater wetland sediments are less certain. Recent experiments in the Florida Everglades showed that salinization led to rapid declines in soil elevation and large soil carbon losses in freshwater and brackish wetlands (Charles et al. 2019), and gradient studies in North Carolina documented reductions in soil respiration and methane emissions during periods of saltwater intrusion (Helton et al. 2019).

We suggest that coastal forested wetland loss represents an important new class of climate change–driven ecological shifts akin to the desertification of drylands (Huang et al. 2016, Berdugo et al. 2020) and the shrubification of arctic tundra (Myers-Smith and Hik 2018, Pastick et al. 2019). Like these other examples, rising water tables and salinization ultimately will shift these formerly freshwater forests into a new ecosystem state (sensu Scheffer 2009), because salinization and sulfidation of soils prevent the regeneration of shrubland back into coastal forests (Munns and Tester 2008, Fagherazzi et al. 2019).

Efforts to forecast the potential for global coastal wetland loss have focused almost entirely on sea-level rise. Schuerch et al. (2018) estimated up to 30% of all coastal wetlands could be subsumed by the sea by 2100. Other recent papers suggest that an even larger proportion of coastal wetlands are vulnerable (Kirwan et al. 2016, Spencer et al. 2016). When we consider the likelihood of wetland loss in the coastal plain interior due to ecosystem salinization, these estimates are likely to increase in magnitude. Perhaps more importantly, considering both salinization and saltwater intrusion will require us to expand our perception of the range of coastal wetland types that are vulnerable to climate change. Our analysis shows that ghost forest formation can be associated with *both* episodic disturbances (i.e., hurricanes) and the gradual progression of sea-level rise and that landscape features such as drainage ditches can increase local vulnerability. We suggest that an analysis of coastal freshwater wetland vulnerability at a global scale is urgently needed. In addition to determining what proportion of interior freshwater forested wetland habitats have already been lost, new remote sensing technologies may enable us to detect vegetation stress and vulnerability prior to forest mortality, that could guide more effective and strategic protection and management.

Acknowledgments

Funding for this research was provided by a NASA Earth and Space Science Fellowship (grant 80NSSC17K0355), the North Carolina Sea Grant/Space Grant (project R/MG-1806), NSF Coastal SEES Collaborative Research (award 1426802), and by Duke University Data+ Program through the Rhodes Information Initiative. We thank D. Urban for help with spatial statistics; our student interns and research assistants, K. Chang, H. Lynch, J. Reeves, and A. Kosinski; and our collaborators at the Alligator River National Wildlife Refuge, especially S. Lanier. Author contributions: EU, JW, and EB conceived of the ideas and project design, EU and XY performed the remote sensing analysis, EU and EB led the writing of the manuscript, and all authors contributed substantially to revising the writing and gave final approval for publication.

Literature Cited

Adam, E., O. Mutanga, and D. Rugege. 2010. Multispectral and hyperspectral remote sensing for identification and mapping of wetland vegetation: A review. Wetlands Ecology and Management 18:281–296.

Asner, G. P. 1998. Biophysical and biochemical sources of variability in canopy reflectance. Remote Sensing of the Environment 64:234–253.

Berdugo, M., et al. 2020. Global ecosystem thresholds driven by aridity. Science 367:787–790.

Bhattachan, A., R. E. Emanuel, M. Ardón, E. S. Bernhardt, S. M. Anderson, M. G. Stillwagon, E. A. Ury, T. K. BenDor, and J. P. Wright. 2018. Evaluating the effects of land-use change and future climate change on vulnerability of coastal landscapes to saltwater intrusion. Elementa: Science of the Anthropocene 6:62.

Bivand, R., T. Keitt, and B. Rowlingson 2019. rgdal: bindings for the 'geospatial' data abstraction library. R package version 1.4-4. https://CRAN.R-project.org/package=rgdal

Blankespoor, B., S. Dasgupta, and B. Laplante. 2014. Sea-level rise and coastal wetlands. Ambio 43:996–1005.

Bojanowski, M., and R. Edwards. 2016. alluvial: R package for creating alluvial diagrams. R package version 0.1-2. https://github.com/mbojan/alluvial

Breiman, L. 2001. Random forests. Machine Learning 45:5–32.

Brinson, M. M. 1991. Landscape properties of pocosins and associated wetlands. Wetlands 1:441–465.

Charles, S. P., et al. 2019. Experimental saltwater intrusion drives rapid soil elevation and carbon loss in freshwater and brackish everglades marshes. Estuaries and Coasts 42:1868–1881.

Church, J. A., et al. 2013. Sea level change. Pages 895–900 *in* T. F. Stocker, D. Qin, G.-K. Plattner, M. Tignor, S. K. Allen, J. Boschung, A. Nauels, Y. Xia, V. Bex, and P. M. Midgley, editors. Climate change 2013: the physical science basis. Contribution of working group I to the fifth assessment report of the intergovernmental panel on climate change. Cambridge University Press, Cambridge, UK.

Cloern, J. E., et al. 2016. Human activities and climate variability drive fast-paced change across the world's estuarine–coastal ecosystems. Global Change Biology 22:513–529.

Desantis, L. R. G., S. Bhotika, K. Williams, and F. E. Putz. 2007. Sea-level rise and drought interactions accelerate forest decline on the Gulf Coast of Florida, USA. Global Change Biology 13:2349–2360.

Douglas, B. C., and W. Richard Peltier. 2002. The puzzle of global sea-level rise. Physics Today 55:35–40.

Duarte, C. M., I. J. Losada, I. E. Hendriks, I. Mazarrasa, and N. Marbà. 2013. The role of coastal plant communities for climate change mitigation and adaptation. Nature Climate Change 3:961–968.

Fagherazzi, S., S. C. Anisfeld, L. K. Blum, E. V. Long, R. A. Feagin, A. Fernandes, W. S. Kearney, and K. Williams. 2019. Sea level rise and the dynamics of the marsh-upland boundary. Frontiers in Environmental Science 7:1–18.

Haer, T., E. Kalnay, M. Kearney, and H. Moll. 2013. Relative sea-level rise and the conterminous United States: Consequences of potential land inundation in terms of population at risk and GDP loss. Global Environmental Change 23:1627–1636.

Helton, A. M., M. Ardón, and E. S. Bernhardt. 2019. Hydrologic context alters greenhouse gas feedbacks of coastal wetland salinization. Ecosystems 22:1108–1125.

Hijmans, R. J. 2019. raster: Geographic data analysis and modeling. R package version 3.0-2. https://CRAN.R-project.org/package=raster

Hillebrand, H., and C. Kunze. 2020. Meta-analysis on pulse disturbances reveals differences in functional and compositional recovery across ecosystems. Ecology Letters 23:575–585.

Holden, J., P. J. Chapman, and J. C. Labadz. 2004. Artificial drainage of peatlands: hydrological and hydrochemical process and wetland restoration. Progress in Physical Geography: Earth and Environment 28:95–123.

Huang, J., H. Yu, X. Guan, G. Wang, and R. Guo. 2016. Accelerated dryland expansion under climate change. Nature Climate Change 6:166–171.

Kennedy, R. E., et al. 2014. Bringing an ecological view of change to Landsat-based remote sensing. Frontiers in Ecology and the Environment 12:339–346.

Kirwan, M. L., and K. B. Gedan. 2019. Sea-level driven land conversion and the formation of ghost forests. Nature Climate Change 9:450–457.

Kirwan, M. L., S. Temmerman, E. E. Skeehan, G. R. Guntenspergen, and S. Fagherazzi. 2016. Overestimation of marsh vulnerability to sea level rise. Nature Climate Change 6:253–260.

Laderman, A. D. 1989. The ecology of Atlantic white cedar wetlands: a community profile. Fish and Wildlife Service, U.S. Department of the Interior, Washington, DC, USA.

Liaw, A., and M. Wiener. 2002. Classification and regression by randomForest. R News 2:18–22.

Manda, A. K., A. S. Giuliano, and T. R. Allen. 2014. Influence of artificial channels on the source and extent of saline water intrusion in the wind tide dominated wetlands of the southern Albemarle estuarine system (USA). Environmental Earth Sciences 71:4409–4419.

Manda, A. K., E. Reyes, and J. M. Pitt. 2018. In situ measurements of wind-driven salt fluxes through constructed channels in a coastal wetland ecosystem. Hydrological Processes 32:636–643.

Meehl, G. A., J. M. Gregory, A. Kitoh, R. Knutti, J. M. Murphy, A. Noda, and Z.-C. Zhao. 2007. Global climate projections. Pages 747–845 *in* S. Solomon, D. Qin, M. Manning, Z. Chen, M. Marquis, K. B. Averyt, M. Tignor, and H. L. Miller, editors. Climate change 2007: the physical science basis. Contribution of working group I to the fourth assessment report of the intergovernmental panel on climate change. Cambridge University Press, Cambridge, UK. http://hdl.handle.net/102.100.100/124551?index=1

Miao, S., C. B. Zou, and D. D. Breshears. 2009. Vegetation responses to extreme hydrological events: sequence matters. American Naturalist 173:113–118.

Munns, R., and M. Tester. 2008. Mechanisms of salinity tolerance. Annual Review of Plant Biology 59:651–681.

Myers-Smith, I. H., and D. S. Hik. 2018. Climate warming as a driver of tundra shrubline advance. Journal of Ecology 106:547–560.

National Oceanic and Atmospheric Administration, Office for Coastal Management. 2010. "C-CAP regional land cover and change" coastal change analysis program (C-CAP) high-resolution land cover. NOAA Office for Coastal Management, Charleston, South Carolina. www.coast.noaa.gov/ccapftp

National Weather Service Advanced Hydrologic Prediction Service. 2016. Pamlico Sound at Oregon Inlet Marina. https://water.weather.gov/ahps2/hydrograph.php?wfo=mhx&gage=orin7

Pastick, N. J., M. T. Jorgenson, S. J. Goetz, B. M. Jones, B. K. Wylie, B. J. Minsley, H. Genet, J. F. Knight, D. K. Swanson, and J. C. Jorgenson. 2019. Spatiotemporal remote sensing of ecosystem change and causation across Alaska. Global Change Biology 25:1171–1189.

Pekel, J. F., A. Cottam, N. Gorelick, and A. S. Belward. 2016. High-resolution mapping of global surface water and its long-term changes. Nature 540:418–422.

Poulter, B. 2005. Interactions between landscape disturbance and gradual environmental change: Plant community migration in response to fire and sea-level rise. Dissertation. Duke University, Durham, North Carolina.

Poulter, B., J. L. Goodall, and P. N. Halpin. 2008. Applications of network analysis for adaptive management of artificial drainage systems in landscapes vulnerable to sea level rise. Journal of Hydrology 357:207–217.

R Development Core Team 2013. R: A language and environment for statistical computing. R Foundation for Statistical Computing, Vienna, Austria. http://www.R-project.org/

Scheffer, M. 2009. Critical transitions in nature and society. Princeton University Press, Princeton, NJ, USA.

Schieder, N. W., and M. L. Kirwan. 2019. Sea-level driven acceleration in coastal forest retreat. Geology 47:1151–1155.

Schuerch, M., et al. 2018. Future response of global coastal wetlands to sea-level rise. Nature 561:231–234.

Spencer, T., M. Schuerch, R. J. Nicholls, J. Hinkel, D. Lincke, A. t. Vafeidis, R. Reef, L. McFadden, and S. Brown. 2016. Global coastal wetland change under sea-level rise and related stresses: The DIVA Wetland Change Model. Global and Planetary Change 139:15–30.

Spivak, A. C., J. Sanderman, J. L. Bowen, E. A. Canuel, and C. S. Hopkinson. 2019. Global-change controls on soil-carbon accumulation and loss in coastal vegetated ecosystems. Nature Geoscience 12:685–692.

Taillie, P. J., C. E. Moorman, B. Poulter, M. Ardón, and R. E. Emanuel. 2019*a*. Decadal-scale vegetation change driven by salinity at leading edge of rising sea level. Ecosystems 22:1918–1930.

Taillie, P. J., C. E. Moorman, L. S. Smart, and K. Pacifici. 2019*b*. Bird community shifts associated with saltwater exposure in coastal forests at the leading edge of rising sea level. PLoS One 14:e0216540.

Tully, K., et al. 2019. The invisible flood: the chemistry, ecology, and social implications of coastal saltwater intrusion. BioScience 69:368–378.

Ury, E. 2021. Rapid deforestation of a coastal landscape driven by sea level rise and extreme events—classified_maps (GeoTIFF). Figshare, data set. https://doi.org/10.6084/m9.figshare.14249912.v1

Ury, E. A., S. M. Anderson, R. K. Peet, E. S. Bernhardt, and J. P. Wright. 2020. Succession, regression and loss: does evidence of saltwater exposure explain recent changes in the tree communities of North Carolina's Coastal Plain? Annals of Botany 125:255–264.

U.S. Fish and Wildlife Service Southeast Region Fire Management Organization. 2011. FY2011 fire division report. https://www.fws.gov/southeast/pdf/report/fire-report-2011.pdf

U.S. Geological Survey. 2019. EROS archive—aerial photography—high resolution orthoimagery (HRO). https://doi.org/10.5066/F73X84W6

Ustin, S. L. 2013. Remote sensing of canopy chemistry. Proceedings of the National Academy of Sciences of the United States of America 110:804–805.

Ustin, S. L., A. A. Gitelson, S. Jacquemoud, M. Schaepman, G. P. Asner, J. A. Gamon, and P. Zarco-tejada. 2009. Remote sensing of environment retrieval of foliar information about plant pigment systems from high resolution spectroscopy. Remote Sensing of Environment 113:S67–S77.

Wasson, K., A. Woolfolk, and C. Fresquez. 2013. Ecotones as indicators of changing environmental conditions: rapid migration of salt marsh-upland boundaries. Estuaries and Coasts 36:654–664.

White, E., and D. Kaplan. 2017. Restore or retreat? Saltwater intrusion and water management in coastal wetlands. Ecosystem Health and Sustainability 3:e01258.

Wickham, H., et al. 2019. Welcome to the tidyverse. Journal of Open Source Software 4:1686.

Yang, L., et al. 2018. A new generation of the United States National Land Cover Database: Requirements, research priorities, design, and implementation strategies. ISPRS Journal of Photogrammetry and Remote Sensing 146:108–123.

Zhang, Y., W. Li, G. Sun, and J. S. King. 2019. Coastal wetland resilience to climate variability: A hydrologic perspective. Journal of Hydrology 568:275–284.

Zhang, Y., W. Li, G. Sun, G. Miao, A. Noormets, R. Emanuel, and J. S. King. 2018. Understanding coastal wetland hydrology with a new regional-scale, process-based hydrological model. Hydrological Processes 32:3158–3173.

Supporting Information

Additional supporting information may be found online at: http://onlinelibrary.wiley.com/doi/10.1002/eap.2339/full

Data Availability

Data (Ury 2021) are available in Figshare. https://doi.org/10.6084/m9.figshare.14249912 Source Landsat images are available from the Earth Engine Data Catalog. https://developers.google.com/earth-engine/datasets/catalog/LANDSAT_LT05_C01_T1_SR; https://developers.google.com/earth-engine/datasets/catalog/LANDSAT_LE07_C01_T1_SR; https://developers.google.com/earth-engine/datasets/catalog/LANDSAT_LC08_C01_T1_SR.